Monthly Notices
of the
ROYAL ASTRONOMICAL SOCIETY

MNRAS **460,** 3992–4002 (2016) doi:10.1093/mnras/stw1266
Advance Access publication 2016 May 31

Common envelope events with low-mass giants: understanding the energy budget

J. L. A. Nandez[1]★ and N. Ivanova[2]★

[1]*SHARCNET, The University of Western Ontario, London, ON N6A 5B7, Canada*
[2]*Department of Physics, University of Alberta, Edmonton AB T6G 2E7, Canada*

Accepted 2016 May 25. Received 2016 May 19; in original form 2015 December 3

ABSTRACT

Common envelope events are important interactions between two binary stars that lead to the formation of close binary systems. We present here a systematic three-dimensional study in which we model common envelope events with low-mass giant donors. The results allow us to revise the energy formalism that is usually used to determine common envelope event outcomes. We show that the energy budget for this type of system should include the recombination energy, and that it also must take into account that a significant fraction of the released orbital energy is taken away by the ejecta. We provide three ways in which our results can be used by binary population synthesis studies: a relation that links the observed post-common envelope binary with the initial binary parameters, a fitting formula for the $\alpha_{\rm ce}\lambda$ parameter of the standard energy formalism, and a revised energy formalism that takes into account both the recombination energy and the energy that is taken away by the ejecta.

Key words: hydrodynamics – binaries: close – subdwarfs – white dwarfs.

1 INTRODUCTION

It is believed that the common envelope event (CEE) is the most important phase in the evolution of a wide range of different types of close binary systems. It most likely plays a crucial role in the formation of X-ray binaries, Type Ia supernova progenitors, double degenerate stars, and more (for a review, see Ivanova et al. 2013a). CEE is a short-lived physical process when two stars orbit inside a single, shared envelope. The outcome of a CEE is either a new binary with a reduced orbit or a merger of the two stars.

One of the standard ways to predict an outcome of a CEE is by using the energy formalism. This method equates the binding energy of the envelope of the donor with the orbital energy before and after the event (see for example van den Heuvel 1976; Webbink 1984):

$$E_{\rm bind} = \Delta E_{\rm orb}\,, \tag{1}$$

where $E_{\rm bind}$ is the binding energy of the envelope of the donor and $\Delta E_{\rm orb}$ is the change in the orbital energy. Recognizing that not all the available orbital energy can be used to eject the envelope of the donor, Livio & Soker (1988) proposed a common envelope efficiency parameter, $\alpha_{\rm CE}$, defined as the fraction of released orbital energy that has been effectively used to eject the envelope of the donor. This $\alpha_{\rm CE}$ parameter is now widely used in binary population synthesis studies (see e.g. Han et al. 2002). A better understanding of the energy budget of a CEE, better than a simple parametrization, could help us to better predict the population of close binaries.

The systems where the parameters of the CEE can be best constrained are double-white-dwarf (DWD) binaries. It is widely believed that the last episode of mass transfer leading to DWD formation was an unstable mass transfer, a CEE, where the donor was a red giant (RG) star (e.g. Tutukov & Yungelson 1981, 1988; Iben & Tutukov 1984; Webbink 1984). For RGs, a well-defined relation between their core masses and radii exists. From the observations of DWD systems, we know that one of the white dwarfs (WDs) is usually younger, and therefore is the remnant of the pre-CE RG donor. However, the mass of the donor cannot be uniquely determined, as long as $\alpha_{\rm CE}$ is uncertain.

In this paper, we perform three-dimensional numerical simulations of CEEs between low-mass RG stars and WD companions. This work is the extension of our preliminary study devoted to the formation of the DWD WD 1101+364 via a CEE (Nandez, Ivanova & Lombardi 2015). Here, we consider a wide parameter space based on the mass of the RG donor, the RG core mass, and the companion mass. Our DWD binaries have a mass ratio $q = M_1/M_2$ between 0.8 and 1.125, where M_1 is the mass of the younger WD (formed during a CEE) and M_2 is the mass of the older WD. The main goal of this paper is to understand the energy budget at the end of the CEE. We pay particular attention to the usage of the recombination energy, and to the energy that is taken away by the ejecta. Those energies are not usually taken into account by the standard energy formalism, and should explain the deviation of $\alpha_{\rm CE}$ from 1.

★E-mail: jnandez@sharcnet.ca (JLAN); nata.ivanova@ualberta.ca (NI)

Table 1. Complete parameter space with initial conditions. The model names are composed of following: two digits representing the RG mass are followed by 'G', three digits representing the RG core mass followed by 'C', three digits representing the old WD mass followed by 'D'; 'S' stands for synchronized case, otherwise the simulation is non-synchronized case. $M_{\rm d,1}$, and $M_{\rm c,1}$ are the total and core mass of the RG, whilst $M_{\rm a,2}$ is the mass of the old WD, in $M_\odot$. $R_{\rm rlof}$ is the radius of the donor Roche lobe, in $R_\odot$. $a_{\rm orb,ini}$ is the initial orbital separation in $R_\odot$, $P_{\rm orb,ini}$ is the initial orbital period in days. $E_{\rm pot,ini}$, $E_{\rm int,ini}$, $E_{\rm bind,ini}$, $E_{\rm rec,ini}$, $E_{\rm orb,ini}$, and $E_{\rm tot,ini}$ are the potential energy of the RG, the internal energy of the RG without recombination, the binding energy of the RG envelope without recombination energy, the total recombination energy of the RG envelope, initial orbital energy, and initial total energy, defined as the sum of the binding, recombination, and initial orbital energies, respectively, in the units of 10^{46} erg. $\lambda \equiv -GM_{\rm d,1}(M_{\rm d,1} - M_{\rm c,1})/(E_{\rm bind,ini}R_{\rm rlof})$ is a dimensionless star structure parameter (de Kool 1990).

Model	$M_{\rm d,1}$	$M_{\rm c,1}$	$M_{\rm a,2}$	$R_{\rm rlof}$	$a_{\rm orb,ini}$	$P_{\rm orb,ini}$	$E_{\rm pot,ini}$	$E_{\rm int,ini}$	$E_{\rm bind,ini}$	$E_{\rm rec,ini}$	$E_{\rm orb,ini}$	$E_{\rm tot,ini}$	λ
1.2G0.32C0.32D	1.195	0.318	0.32	29.484	59.47	43.11	−24.542	12.214	−12.328	2.725	−1.218	−10.825	1.093
1.2G0.32C0.36D	1.195	0.318	0.36	29.484	60.74	44.00	−24.542	12.214	−12.328	2.725	−1.345	−10.945	1.093
1.2G0.32C0.40D	1.195	0.318	0.40	29.484	61.93	44.65	−24.542	12.214	−12.328	2.725	−1.462	−11.066	1.093
1.4G0.32C0.32D	1.397	0.319	0.32	27.735	54.47	35.52	−33.772	16.825	−16.947	3.369	−1.556	−15.134	1.217
1.4G0.32C0.36D	1.397	0.319	0.36	27.735	55.59	36.24	−33.772	16.825	−16.947	3.369	−1.715	−15.293	1.217
1.4G0.32C0.40D	1.397	0.319	0.40	27.735	56.64	36.82	−33.772	16.825	−16.947	3.369	−1.870	−15.456	1.217
1.6G0.32C0.32D	1.598	0.323	0.32	25.805	49.57	29.21	−45.768	22.931	−22.837	4.009	−1.955	−20.783	1.312
1.6G0.32C0.36D	1.598	0.323	0.36	25.805	50.54	29.76	−45.768	22.931	−22.837	4.009	−2.157	−20.985	1.312
1.6G0.32C0.36D-S	1.598	0.323	0.36	31.250	48.61	27.97	−44.769	22.412	−22.357	3.997	−2.241	−20.602	1.106
1.6G0.32C0.40D	1.598	0.323	0.40	25.805	51.48	30.29	−45.768	22.931	−22.837	4.009	−2.353	−21.181	1.312
1.8G0.32C0.32D	1.799	0.318	0.32	16.336	30.77	13.59	−88.123	43.955	−44.167	4.676	−3.544	−43.036	1.401
1.8G0.32C0.36D	1.799	0.318	0.36	16.336	31.37	13.86	−88.123	43.955	−44.167	4.676	−3.912	−43.404	1.401
1.8G0.32C0.40D	1.799	0.318	0.40	16.336	31.93	14.10	−88.123	43.955	−44.167	4.676	−4.271	−43.762	1.401
1.2G0.36C0.32D	1.177	0.362	0.32	60.088	121.63	127.06	−13.403	6.649	−6.754	2.479	−0.587	−4.861	0.896
1.2G0.36C0.36D	1.177	0.362	0.36	60.088	124.24	129.46	−13.403	6.649	−6.754	2.479	−0.646	−4.921	0.896
1.2G0.36C0.40D	1.177	0.362	0.40	60.088	126.68	131.59	−13.403	6.649	−6.754	2.479	−0.704	−4.979	0.896
1.4G0.36C0.32D	1.383	0.364	0.32	56.700	111.58	104.66	−18.200	9.103	−9.097	3.135	−0.752	−6.713	1.037
1.4G0.36C0.36D	1.383	0.364	0.36	56.700	113.88	106.68	−18.200	9.103	−9.097	3.135	−0.829	−6.790	1.037
1.4G0.36C0.40D	1.383	0.364	0.40	56.700	116.04	108.49	−18.200	9.103	−9.097	3.135	−0.906	−6.865	1.037
1.6G0.36C0.32D	1.592	0.363	0.32	50.061	96.21	79.10	−25.439	12.700	−12.739	3.830	−1.003	−9.914	1.163
1.6G0.36C0.36D	1.592	0.363	0.36	50.061	98.13	80.64	−25.439	12.700	−12.739	3.830	−1.107	−10.017	1.163
1.6G0.36C0.40D	1.592	0.363	0.40	50.061	99.93	82.03	−25.439	12.700	−12.739	3.830	−1.208	−10.118	1.163
1.8G0.36C0.32D	1.796	0.360	0.32	41.147	77.51	54.32	−37.269	18.684	−18.585	4.521	−1.405	−15.469	1.279
1.8G0.36C0.36D	1.796	0.360	0.36	41.147	79.01	55.38	−37.269	18.684	−18.585	4.521	−1.551	−15.614	1.279
1.8G0.36C0.40D	1.796	0.360	0.40	41.147	80.42	56.35	−37.269	18.684	−18.585	4.521	−1.693	−15.756	1.279

We describe the initial conditions, the parameter space and the numerical methods in Section 2. Section 3 contains the definitions for the energies. In Section 4, we give an overview of the final states of the simulations in terms of the mass of the ejecta, energy evolution during a spiral-in, orbital parameters at the end of a CEE, and discuss how the outcomes of the CEE can be parametrized. Finally, Section 5 gives a brief discussion on how our results can be used in population synthesis studies, as well as comparison with the observed binaries that are known to have a post-CE WD.

2 PARAMETER SPACE

We study the progenitor systems that have likely formed the observed DWDs, in terms of the observed WD masses and the orbital separations. We adopt that immediately before a CEE, the DWD progenitor binaries consisted of a low-mass RG with a core mass close to the observed new (second-formed) WD and of an older (first-formed) WD. We consider 24 binaries in the parameter space defined by the RG donor mass, the mass of the newly formed WD (RG core), and the mass of the old WD. For the RG donor mass, $M_{\rm d,1}$, we take 1.2, 1.4, 1.6, and 1.8 $M_\odot$. Each low-mass RG is considered at two evolutionary points on its RG branch, namely when their degenerate He core masses $M_{\rm c,1}$ are 0.32 and 0.36 $M_\odot$ cores (we expect that the mass of the new WD will be very similar to the He core mass of the RG donors). For the mass of the old WD, $M_{\rm a,2}$, we take 0.32, 0.36, and 0.40 $M_\odot$, for each case of the RG donor. Table 1 shows the summary of the considered parameter space, and the initial conditions for each binary.

To create the initial RG donor stars, we use the TWIN/EV stellar code (Eggleton 1971, 1972, recent updates are described in Glebbeek, Pols & Hurley 2008). This allows us to obtain a realistic initial one-dimensional (1D) stellar profile for each RG donor. Stars are evolved until their degenerate He cores have grown close to 0.32 and 0.36 $M_\odot$. To model a CEE between an RG and a WD, we use STARSMASHER (Gaburov, Lombardi & Portegies Zwart 2010; Lombardi et al. 2011), a smoothed particle hydrodynamics (SPH) code. Technical details on using this code to model CEEs can be found in Nandez, Ivanova & Lombardi (2014). We reiterate the point made in Nandez et al. (2015), that when a 1D star is transferred to a 3D code via the *relaxation* process in STARSMASHER, the core of the RG, $M_{\rm c,1}$, must be increased slightly by about 0.01 $M_\odot$ so that the resulting profile of the 3D star for pressure, density, internal energy, and other quantities would match that of a 1D star. The RG envelope is modelled using 10^5 particles, and the RG core is modelled as a point mass, as is the WD (note that a point mass only interacts gravitationally with normal SPH particles). The envelope mass in our three-dimensional star is $M_{\rm env,1} = M_{\rm d,1} - M_{\rm c,1}$. We found that for most RGs with cores close to 0.4 $M_\odot$, the profiles could not be matched well with 1D stars after the relaxation, and hence RGs with core masses >0.4 $M_\odot$ were excluded from the considered parameter space. Improving the match of the profiles in those more evolved donors is computationally unfeasible now, as this requires such a change in the number of SPH particles and in their

smoothing length, that the GPU time would be increased by at least 64 times.[1]

The photospheric radius of the star in SPH, $R_{\rm SPH}$, is defined as $R_{\rm SPH} = R_{\rm out} + 2h_{\rm out}$, where $R_{\rm out}$ is the position of the outermost particle and $h_{\rm out}$ is the smoothing length of that particle (for a detailed discussion on how to define the photospheric radius of a three-dimensional star, see Nandez et al. 2014). Defining the photospheric radius this way ensures that all envelope particles are enclosed within $R_{\rm SPH}$ for the non-synchronized cases.

The initial orbital separation, $a_{\rm orb,ini}$, for the non-synchronized cases is found from the assumption that $R_{\rm SPH}$ is equal to the Roche lobe (RL) radius, $R_{\rm rl}$, and using the approximation for the RL radius by Eggleton (1983). The initial orbital period, $P_{\rm orb,ini}$, is found assuming a Keplerian orbit.

For the synchronized case, the initial orbital period and separation are found at the moment when the outermost particles overfill the donor's RL during the *scan* process (see section 2.3 of Lombardi et al. 2011, also Nandez et al. 2015). During the scan process, the envelope's angular momentum is steadily boosted. This leads to the expansion of the radius of the donor as compared to the non-rotating case. As a result, the orbital separation in a synchronized and a non-synchronized case may not match; however, the difference in these quantities is not large. The photospheric radius is $R_{\rm SPH} = R_{\rm out}$ for the synchronized case.

We use the tabulated equation of state (TEOS) incorporated from MESA (see section 4.2 of Paxton et al. 2011) and implemented as described in Nandez et al. (2015). This TEOS includes recombination energy for H, He, C, N, O, Ne, and Mg. The dominant contribution to the recombination energy comes from H, which account for about 59 per cent of the total energy, followed by He with about 38 per cent, and 3 per cent for the rest of the elements, in all our simulations.

3 DEFINITIONS

In this section, we declare definitions for the most important quantities. Definitions are adopted from Nandez et al. (2015), unless stated otherwise.

Energy formalism. The energy formalism compares the donor's envelope binding energy $E_{\rm bind}$ with the orbital energy before the CEE, $E_{\rm orb,ini}$, and after the CEE, $E_{\rm orb,fin}$ (Webbink 1984; Livio & Soker 1988):

$$E_{\rm bind} = \alpha_{\rm bind}(E_{\rm orb,fin} - E_{\rm orb,ini}) \equiv \alpha_{\rm bind}\Delta E_{\rm orb}\,. \tag{2}$$

Here $\alpha_{\rm bind}$ is the fraction of the orbital energy effectively used to expel the CE. This parameter is equivalent to the commonly used $\alpha_{\rm CE}$, and is usually assumed to be $0 \leq \alpha_{\rm bind} \leq 1$.

The potential energy of the donor's envelope in SPH is

$$E_{\rm pot,ini} = \frac{1}{2}\sum_i m_i\phi_i, \tag{3}$$

where m_i and ϕ_i are the mass and specific gravitational energy, respectively, for each SPH particle i in the initial RG profile, including the core. Note that this quantity is computed before the star is placed in the binary configuration. In our SPH method, ϕ_i is calculated as in Hernquist & Katz (1989).

[1] The average time that is spent on obtaining one model presented in this paper is about 1 GPU core year. The global GPU resource available at Compute/Calcul Canada for all scientists in Canada, in several GPU-equipped clusters, is about 200 GPU core years.

The internal energy of the donor's envelope in SPH is

$$E_{\rm int,ini} = \sum_i m_i\left(\frac{3}{2}\frac{kT_i}{\mu_i m_{\rm H}} + \frac{aT_i^4}{\rho_i}\right), \tag{4}$$

where T_i, ρ_i, and μ_i are the temperature, density, and mean molecular mass, respectively, for each particle i in the initial RG profile. The constants k, a, and $m_{\rm H}$ are the Boltzmann constant, radiation constant, and hydrogen atom mass.

The binding energy of the RG, without the recombination energy, is

$$E_{\rm bind} = E_{\rm pot,ini} + E_{\rm int,ini}. \tag{5}$$

This binding energy was historically parametrized using the parameter λ (de Kool 1990; Ivanova et al. 2013a),

$$E_{\rm bind} = -\frac{GM_{\rm d,1}(M_{\rm d,1} - M_{\rm c,1})}{\lambda R}. \tag{6}$$

This equation, combined with the energy formalism equation (2), provides the most used equation to find CEE outcomes in binary population synthesis studies, where $\alpha_{\rm bind}\lambda$ are used together as one single parameter:

$$\Delta E_{\rm orb} = -\frac{GM_{\rm d,1}(M_{\rm d,1} - M_{\rm c,1})}{\alpha_{\rm bind}\lambda R}. \tag{7}$$

The orbital energy of the binary system in SPH takes the following form:

$$E_{\rm orb} = \frac{1}{2}\mu|\boldsymbol{V}_{12}|^2 + \frac{1}{2}\sum_i m_i\phi_i - \frac{1}{2}\sum_j m_j\phi_j^{\rm RL_1} - \frac{1}{2}\sum_k m_k\phi_k^{\rm RL_2}, \tag{8}$$

where $\mu = M_1M_2/(M_1 + M_2)$ is the reduced mass, and $\boldsymbol{V}_{12} = \boldsymbol{V}_1 - \boldsymbol{V}_2$ is the relative velocity of the two stars. The first, second, third, and fourth terms give the orbital kinetic energy, the total gravitational energy of the binary (with the sum being over all particles i in the binary), the self-gravitational energy of the donor (the sum being over all particles j in star 1), and of the WD (the sum being over all particles k in star 2, initially just the one particle representing the WD), respectively.

Recombination energy. The recombination energy is included in the total value of the specific internal energy provided by TEOS, and can be found as

$$E_{\rm rec,ini} = \sum_i m_i\left(u_i - \frac{3}{2}\frac{kT_i}{\mu_i m_{\rm H}} - \frac{aT_i^4}{\rho_i}\right) \equiv \alpha_{\rm rec}\Delta E_{\rm orb}, \tag{9}$$

where u_i is the SPH specific internal energy for each particle. $\alpha_{\rm rec}$ is the ratio between the recombination energy and the released orbital energy. Since the recombination energy acts as an additional (to the orbital energy) source of energy, $\alpha_{\rm rec} < 0$. This energy is not part of the usually considered binding energy, as it is not available immediately, and its release must be triggered (Ivanova, Justham & Podsiadlowski 2015). The amount of stored recombination energy is proportional to the mass of the envelope $E_{\rm rec,ini} = \eta(M_{\rm d,1} - M_{\rm c,1})$. In a fully ionized gas that consists of only helium (0.3 mass fraction) and hydrogen (0.7 mass fraction), $\eta \simeq 1.5 \times 10^{13}$ erg g^{-1}. Our gas chemical composition is a bit different, and also our TEOS takes ionization of heavier elements into account as well. For our donors, we find $\eta \simeq 1.6 \times 10^{13}$ erg g^{-1}. The version of STARSMASHER we use evolves, for each SPH particle, the specific internal energy u_i and density ρ_i (see equations A18 and A7 of Gaburov et al. 2010). The

pressure is then found from the internal energy, density, and the adopted equation of state.

Total energy. The total initial energy, $E_{\rm tot,ini}$, is

$$E_{\rm tot,ini} = E_{\rm orb,ini} + E_{\rm bind} + E_{\rm rec}. \quad (10)$$

This quantity is conserved during the evolution of all our models.

Bound and unbound material. For each particle, its total energy is defined as $E_{{\rm tot},i} \equiv 0.5 m_i v_i^2 + m_i \phi_i + m_i u_i$, where the first, second, and third terms are the kinetic, potential, and internal energies, respectively. We classify our particle as in Nandez et al. (2015):

(i) the *ejecta*, $m_{\rm unb}$ – the particles that have positive energy,
(ii) the *circumbinary* material, $m_{\rm cir}$ – the matter that is bound to the binary, but is located outside of both RLs, and
(iii) the *binary* material, $m_{\rm bin}$ – the particles that are inside either of the two RLs.

The total energy of the unbound material at infinity is found when the unbound mass is in a steady state after the CEE. It is computed as

$$E^{\infty}_{\rm tot,unb} = \sum_i E^{\rm unb}_{\rm tot,i} \equiv -\alpha^{\infty}_{\rm unb} \Delta E_{\rm orb}\,. \quad (11)$$

Note that $E^{\rm unb}_{\rm tot,i}$ includes the recombination energy of the unbound material. $\alpha^{\infty}_{\rm unb}$ is the ratio of the energy taken away by the unbound material to the released orbital energy.

Final energies. The total energy at the end of the simulation is distributed in the 'binding' energy of the gas bound to the binary, $E_{\rm bind,fin}$, the final orbital energy of the binary, $E_{\rm orb,fin}$, and the total energy of the unbound material at infinity, $E^{\infty}_{\rm tot,unb}$:

$$E_{\rm tot,fin} = E_{\rm orb,fin} + E_{\rm bind,fin} + E^{\infty}_{\rm tot,unb}, \quad (12)$$

where $E^{\infty}_{\rm tot,unb}$ is composed of $E^{\infty}_{\rm kin,unb}$, $E^{\infty}_{\rm int,unb}$, and $E^{\infty}_{\rm pot,unb}$ – the kinetic, internal, and potential energies of the unbound material, respectively.

Generally, $E_{\rm bind,fin}$ has a fairly small absolute value at the end of the simulation, and so can be safely disregarded. In addition, the particles around the WD may be accreted during a CEE, and hence their presence there may not have any physical meaning. The extended energy formalism, following to Nandez et al. (2015), can then be written as follows:

$$\alpha_{\rm bind} + \alpha_{\rm rec} + \alpha^{\infty}_{\rm unb} \approx 1. \quad (13)$$

If $\alpha_{\rm rec} = \alpha^{\infty}_{\rm unb} = 0$, then equation (13) reduces to the standard energy formalism.

For additional analysis of the energies at the end of a CEE, we introduce three more quantities:

(i) $\alpha_{\rm pot} \equiv E^{\infty}_{\rm pot,unb}/E_{\rm pot,ini}$ – the ratio of the potential energy taken away by the ejecta to the initial potential energy of the RG envelope,
(ii) $\alpha_{\rm th} \equiv E^{\infty}_{\rm int,unb}/(E_{\rm int,ini} + E_{\rm rec})$ – the ratio of the internal energy (including recombination) taken away by the ejecta to the sum of the initial internal energy and the recombination energy of the RG envelope,
(iii) $\alpha^{\infty}_{\rm kin} \equiv -E^{\infty}_{\rm kin,unb}/\Delta E_{\rm orb}$ – the ratio of the kinetic energy taken away by the ejecta to the released orbital energy.

We point out that $\alpha^{\infty}_{\rm kin}$ is a part of $\alpha^{\infty}_{\rm unb}$; however, $\alpha_{\rm pot}$ and $\alpha_{\rm th}$ are not a part of $\alpha^{\infty}_{\rm unb}$ as they describe fractions of their corresponding initial energies.

All our simulations conserved quite well the total angular momentum and the total energy. We have checked and found that the error in the energy conservation in all our simulations is less than 0.1 per cent of the initial total energy, while the error in the angular momentum conservations in all our non-synchronized cases is less than 0.001 per cent of the initial total angular momentum value, and the error in the angular momentum conservation in the only synchronized case is 0.4 per cent.

4 RESULTS

4.1 Overview

Masses. At the end of each simulation, we form a binary consisting of M_1 and M_2 (see Table 2). We note that M_1 and M_2 in Table 2 differ from the values given for $M_{\rm c,1}$ and $M_{\rm a,2}$ in Table 1, respectively, as a few SPH gas particles remain within the RLs of the DWD binary. Ultimately, the ejected material $M_{\rm unb}$ is at least 99.4 per cent of the initial RG envelope, and there is no circumbinary matter around the newly formed DWD binary.

Final time. We stop our simulations no less than 800 orbits after the end of the plunge-in, and typically we stop the simulations after more than 2000 orbits. The plunge-in is the fastest phase of the spiral-in, during which the instantaneous separation (distance) between the RG core and the WD changes substantially on the time-scale comparable to its inferred orbital period. At the moment we stop, the orbital separation is changing by less than $|\delta a_{\rm orb}/a_{\rm orb}| < 0.002$, where $\delta a_{\rm orb}$ is found over one binary orbital period. Some simulations were calculated for much longer, e.g. the case 1.8G0.32C0.36D is calculated for more than 10 000 orbits after the end of the plunge-in, and the change of the orbital separation over the binary orbital period, at the end of the simulation, is $|\delta a_{\rm orb}/a_{\rm orb}| \approx 0.0002$. The final parameters provided in Table 2 are expected to be time-converged values.

Energies. Fig. 1 shows how the energies change during the spiral-in phase for the case 1.2G0.32C0.32D. After the spiral-in phase is complete and there is no circumbinary matter left, the circumbinary total energy vanishes, while the ejecta energy and binary total energy (which is the orbital energy plus the 'binding' energy of the remaining particles) converge to their final values. Table 2 provides the final distributions of energies for all our simulations. Some ostensible deviations can be observed in Table 2. For example, the model 1.8G0.32C0.32D has more energetic ejecta than other models. We note that the overall energy budget, and the energy that was extracted from the formed binary, is much higher in this model than in any other model.

4.2 Role of the recombination energy

In brief, we found that the circumbinary recombination energy has a maximum during the plunge-in phase. At this moment, almost the entire envelope is no longer within the RL of the binary and becomes circumbinary material (see an example in Fig. 2). The ejection of the circumbinary envelope then takes place on its dynamical time-scale, which, e.g. for the case 1.2G0.32C0.32D, is about 100 d.

Let us consider in detail why the dominant energy source that drives the final ejection of the puffed-up envelope is the recombination energy but not the binary orbital energy. For that, we will trace the evolution of *specific energies* during the crucial time at about the plunge-in, when the puffed-up circumbinary envelope formed initially.

The binary orbital energy can be expected to boost the envelope's ejection by being transferred into kinetic energy of the envelope. However, the acceleration of material by the binary's motion, which also can be called a dynamical tide, will only affect the mass that is

Table 2. Energies and masses. $M_{\rm unb}$, M_1, and M_2 are the unbound, stripped RG core, and old WD, in $M_\odot$. $E^{\infty}_{\rm kin,unb} = \sum_i m_i^{\rm unb} v_i^2/2$, $E^{\infty}_{\rm int,unb} = \sum_i m_i^{\rm unb} u_i$, $E^{\infty}_{\rm pot,unb} = \sum_i m_i^{\rm unb} \phi_i$, and $E^{\infty}_{\rm tot,unb}$ are kinetic, internal, potential, and total energies, respectively, for the unbound material. $E_{\rm orb,fin}$ is the orbital energy after the CEE. $E_{\rm bind,fin}$ is the total energy of the particles that remained bound to the binary. $E_{\rm tot,fin}$ is the total energy of all the particles, and $\Delta E_{\rm orb}$ is the released orbital energy. All energies are in 10^{46} erg.

Model	$M_{\rm unb}$	M_1	M_2	$E^{\infty}_{\rm kin,unb}$	$E^{\infty}_{\rm int,unb}$	$E^{\infty}_{\rm pot,unb}$	$E^{\infty}_{\rm tot,unb}$	$E_{\rm orb,fin}$	$E_{\rm bind,fin}$	$E_{\rm tot,fin}$	$\Delta E_{\rm orb}$
1.2G0.32C0.32D	0.870	0.324	0.320	4.827	0.757	−0.044	5.539	−15.653	−0.712	−10.826	−14.308
1.2G0.32C0.36D	0.872	0.323	0.360	4.604	0.629	−0.041	5.192	−15.504	−0.639	−10.951	−14.159
1.2G0.32C0.40D	0.872	0.323	0.400	7.094	1.182	−0.069	8.206	−18.847	−0.430	−11.071	−17.385
1.4G0.32C0.32D	1.074	0.323	0.320	3.733	1.490	−0.218	5.006	−19.638	−0.510	−15.142	−18.082
1.4G0.32C0.36D	1.079	0.319	0.360	6.790	0.907	−0.094	7.603	−22.911	−0.005	−15.313	−21.196
1.4G0.32C0.40D	1.074	0.323	0.400	5.797	1.688	−0.248	7.237	−22.329	−0.364	−15.456	−20.459
1.6G0.32C0.32D	1.271	0.323	0.324	4.212	2.030	−0.475	5.767	−26.153	−0.406	−20.792	−24.198
1.6G0.32C0.36D	1.274	0.323	0.362	6.074	1.044	−0.155	6.964	−27.814	−0.145	−20.995	−25.657
1.6G0.32C0.36D-S	1.274	0.323	0.362	6.205	0.686	−0.093	6.798	−27.292	−0.145	−20.639	−25.051
1.6G0.32C0.40D	1.274	0.323	0.401	7.115	1.316	−0.205	8.226	−29.273	−0.140	−21.187	−26.920
1.8G0.32C0.32D	1.481	0.318	0.320	8.753	3.532	−1.277	11.008	−53.454	−0.621	−43.067	−49.910
1.8G0.32C0.36D	1.478	0.318	0.362	8.333	1.675	−0.371	9.637	−52.873	−0.171	−43.407	−48.961
1.8G0.32C0.40D	1.479	0.318	0.402	7.990	2.755	−0.934	9.811	−53.115	−0.729	−43.768	−48.609
1.2G0.36C0.32D	0.808	0.370	0.320	2.652	0.693	−0.042	3.303	−7.641	−0.526	−4.864	−7.054
1.2G0.36C0.36D	0.808	0.368	0.360	1.896	0.985	−0.089	2.792	−7.200	−0.514	−4.922	−6.554
1.2G0.36C0.40D	0.808	0.369	0.400	3.811	0.449	−0.021	4.239	−8.781	−0.437	−4.979	−8.077
1.4G0.36C0.32D	1.013	0.370	0.320	2.863	0.886	−0.074	3.675	−9.963	−0.428	−6.716	−9.211
1.4G0.36C0.36D	1.013	0.370	0.360	2.498	1.282	−0.141	3.639	−9.994	−0.437	−6.792	−9.165
1.4G0.36C0.40D	1.013	0.371	0.400	2.842	1.155	−0.109	3.888	−10.249	−0.508	−6.869	−9.343
1.6G0.36C0.32D	1.229	0.363	0.320	4.111	0.904	−0.067	4.948	−14.851	−0.013	−9.916	−13.848
1.6G0.36C0.36D	1.222	0.363	0.360	4.009	1.766	−0.238	5.537	−15.512	−0.047	−10.022	−14.405
1.6G0.36C0.40D	1.224	0.368	0.400	3.773	1.687	−0.226	5.234	−14.993	−0.366	−10.125	−13.785
1.8G0.36C0.32D	1.436	0.360	0.320	3.990	2.392	−0.425	5.957	−21.233	−0.195	−15.471	−19.828
1.8G0.36C0.36D	1.436	0.360	0.360	4.407	3.700	−1.371	6.735	−21.727	−0.623	−15.615	−20.176
1.8G0.36C0.40D	1.433	0.360	0.403	4.852	2.258	−0.448	6.661	−22.047	−0.380	−15.766	−20.354

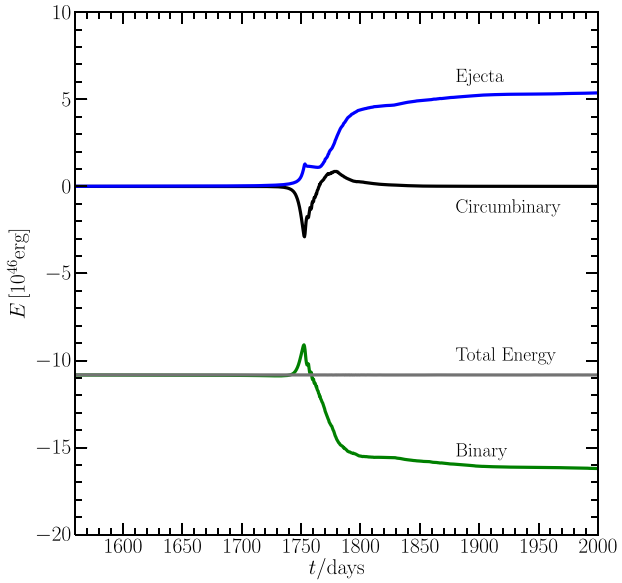

Figure 1. The evolution of the total energy (grey solid line), the orbital energy $E_{\rm orb}$ (green solid line), the energy in the circumbinary matter (black solid line), and the energy in the ejecta (blue solid line) for the case 1.2G0.32C0.32D.

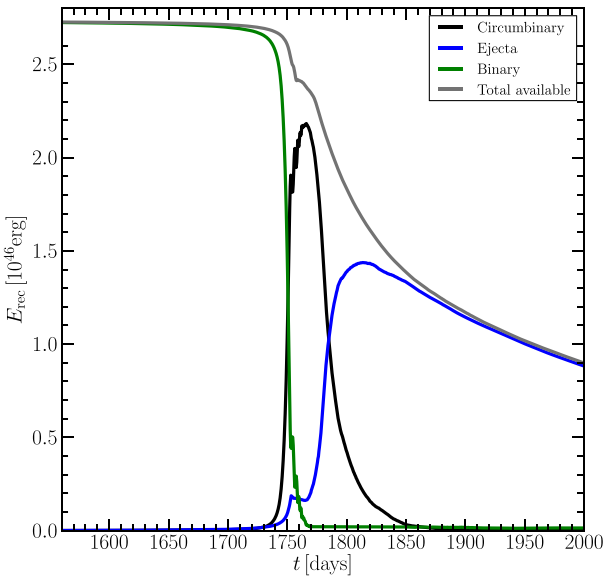

Figure 2. The evolution of the total recombination energy (grey solid line), the recombination energy in SPH particles bound to the binary (green solid line), the recombination energy in SPH particles in the circumbinary material (black solid line), and the recombination energy in the ejecta (blue solid line), shown for the case 1.2G0.32C0.32D.

located approximately within three binary orbital separations of the binary's centre of mass (see e.g. Portegies Zwart & Meinen 1993). Note that we do not consider here any secular tidal effects, but only an acceleration that is produced during a period of time that is less than a hundred orbital periods of the binary after the plunge-in, i.e. comparable to when the envelope is ejected in our simulations. We can test whether the mass located far away from the binary is, or is not, accelerated by the binary in our case.

First, we separate the bound envelope into two sub-envelopes: the inner envelope – the envelope's mass that is within the distance of $3a_{\rm orb}$, $m_{\rm bound,\,tid}$ – and the outer envelope, $m_{\rm bound,\,notid}$, or the mass

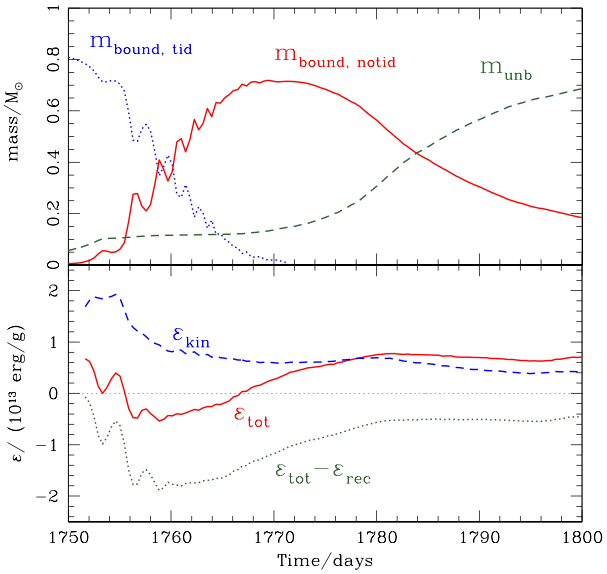

Figure 3. The evolution of the specific energies and the masses for the case 1.2G0.32C0.32D. The bottom plot shows the specific energies per unit mass in the outer envelope (see Section 4.2): kinetic energy $\varepsilon_{\rm kin}$, total energy including recombination $\varepsilon_{\rm tot}$, and total energy excluding recombination $\varepsilon_{\rm tot} - \varepsilon_{\rm rec}$. See the text in Section 4.2 for details on masses.

that is beyond $3a_{\rm orb}$. Here $a_{\rm orb}$ is the current distance between the RG core and the WD. The outer envelope, once it is 'decoupled' from the binary's tidal effect, is expected to evolve according to its potential, kinetic, internal, and recombination energies.

Let us consider the case 1.2G0.32C0.32D (see Fig. 3). In the evolution shown, the plunge-in takes place from days 1750 to 1770, when the orbital separation shrinks by a factor of 10, approaching closely its final value. At day 1770, most of the initial envelope is either in the outer envelope or is ejected. During the plunge-in, the definition of the orbital separation $a_{\rm orb}$ by the energetic principle cannot provide a proper result (for the energy budget and the orbital separation ambiguity during the plunge-in, see Ivanova & Nandez 2016); hence, we can only use a geometrical distance between the RG core and WD. During the plunge-in, the inferred orbital separation is changing rapidly (in a sense, it can also be described as having a very high eccentricity). Since the boundary between the outer and inner envelopes, drawn at $3a_{\rm orb}$, oscillates as well as the orbital separation itself, the defined masses of the envelopes and their energies oscillate during the plunge-in.

In Fig. 3, we can see that the specific kinetic energy of the outer envelope is settled by the end of the plunge-in. This outer envelope is bound by the conventional definition, in which the total energy excluding recombination is negative. At the same time, the outer envelope is effectively decoupled from the binary and is not receiving further boosts to its kinetic energy.

At the moment of the end of the plunge-in, the outer envelope possesses most of the mass that remains bound to the binary. The outer envelope has obtained some kinetic energy from its previous interaction with the shrinking binary during the plunge-in. That non-zero kinetic energy leads to the envelope expansion, on the dynamical time-scale of the expanded envelope, where every SPH particle in the outer envelope can have only a parabolic (bound) trajectory with respect to the binary, if the recombination energy is not released.

However, once the material expands and cools down enough to start recombination, an SPH particle gains enough energy to become unbound – it can be seen from Fig. 3 that at the end of the plunge-in, the stored potential recombination energy is sufficient to unbind the material of the outer envelope. The outer envelope is now flowing away; as more of its material feels a pressure differential between open space above and the remaining envelope below, it expands further, cools down, and becomes unbound after recombination. This recombination-driven ejection is gradual and non-explosive, versus the rather explosive, or dynamical, ejection that takes place during the plunge-in, as described in detail by Ivanova & Nandez (2016). The radius at which the released recombination energy can remove a particle out of the potential well is the 'recombination' radius, and was derived in Ivanova & Nandez (2016). We can clarify that there is no recombination energy stored in the ejected material at the end of the simulations.

It is important to mention that the recombination takes place at large optical depths. Using our 3D models, we estimate that typical optical depths have values of at least 10, and 1D studies showed that hydrogen recombination can take place at optical depths above 100 (Ivanova et al. 2015).

4.3 Post-CE orbital parameters

We find the final orbital separation in a *geometrical way* as $a_{\rm orb,fin} = (r_{\rm a} + r_{\rm p})/2$, where $r_{\rm p}$ is the periastron and $r_{\rm a}$ is the apastron. We ensure that these two quantities, $r_{\rm p}$ and $r_{\rm a}$, are no longer changing with time at the moment when we extract them from the simulations. We find the final orbital period of the binary assuming a Keplerian orbit, $P_{\rm orb,fin}$. Another important orbital parameter is the eccentricity, e, which is found as $e = (r_{\rm a} - r_{\rm p})/(2a_{\rm orb,fin})$. The final orbital parameters are provided in Table 3.

Note that the final separation found using the orbital energy, $a^{\rm En}_{\rm orb,fin} = -GM_1M_2/(2E_{\rm orb,fin})$, differs from the final orbital separation found in the geometric way, $a_{\rm orb,fin}$. This is for two reasons.

(i) There is still mass within the RLs of both point masses, as can be seen by the non-zero value of $E_{\rm bind,fin}$. The presence of these particles, and their not fully stable orbits around the point masses, makes the energy-based way to calculate $a^{\rm En}_{\rm orb,fin}$ uncertain. Note that these few particles make the stars aspherical and the equation for $a^{\rm En}_{\rm orb,fin}$ is formally not valid.

(ii) The distance between the two point masses (WD and RG core) is less than two times their smoothing lengths, which means that there is some extra smoothing in the gravitational potential equation (see the appendix of Hernquist & Katz 1989). The smoothing length of the point masses acts as the softening term defined by Hernquist & Katz (1989). For details on the definition and how to determine the smoothing length in the case modelled here, see Lombardi et al. (2011). As an example, in the model 1.8G0.32C0.32D, the smoothing length for the RG core is $h_{\rm core} = 0.35\,{\rm R}_\odot$, and the smoothing length for the WD is $h_{\rm WD} = 0.73\,{\rm R}_\odot$.

The difference in orbital separations between the geometrical way $a_{\rm orb,fin}$ and the energy way $a^{\rm En}_{\rm orb,fin}$ varies from 7.19 per cent (1.2G0.32C0.36D) to 18.11 per cent (1.8G0.32C0.32W), where the separation derived via the geometrical way is always smaller than the separation derived via the energy way. There is a very small discrepancy for the initial orbital separations using the two methods, <0.24 per cent.

The two values for the orbital separation would be closer to each other if the potential in the SPH code were calculated without a softening term. Note however that due to the first reason above, which is the presence of SPH particles inside the RLs, the two terms will never be completely the same. The discrepancy between

Table 3. Orbital parameters. The closest and farthest orbital separations are r_p and r_a, respectively, while $a_{orb,fin}$ is the semimajor axis (all in $R_\odot$). The orbital period $P_{orb,fin}$ is given in days, and e is the eccentricity of the orbit. The energy fractions α_{bind}, α_{rec}, and α^{∞}_{unb} are defined in equations (2), (9), and (11), respectively. α_{pot} is the fraction of potential energy taken by the ejecta with respect to the initial potential energy. α_{th} is the ratio of the thermal energy taken by the ejecta to the initial thermal energy (including recombination energy), and α^{∞}_{kin} is the kinetic energy scaled with the released orbital energy.

Model	r_p	r_a	$a_{orb,fin}$	$P_{orb,fin}$	e	α_{bind}	α_{rec}	α^{∞}_{unb}	α_{pot}	α_{th}	α^{∞}_{kin}	$\alpha_{bind}\lambda$
1.2G0.32C0.32D	1.342	1.415	1.379	0.234	0.026	0.856	−0.189	0.384	0.003	0.064	0.323	0.936
1.2G0.32C0.36D	1.520	1.532	1.526	0.264	0.004	0.871	−0.192	0.367	0.002	0.042	0.325	0.952
1.2G0.32C0.40D	1.415	1.422	1.419	0.230	0.002	0.709	−0.157	0.472	0.003	0.079	0.408	0.775
1.4G0.32C0.32D	1.093	1.153	1.123	0.172	0.027	0.937	−0.186	0.277	0.006	0.074	0.206	1.140
1.4G0.32C0.36D	1.070	1.089	1.080	0.158	0.009	0.800	−0.159	0.359	0.003	0.045	0.320	0.974
1.4G0.32C0.40D	1.197	1.243	1.220	0.184	0.019	0.828	−0.165	0.354	0.007	0.084	0.283	1.008
1.6G0.32C0.32D	0.848	0.882	0.865	0.116	0.020	0.944	−0.166	0.238	0.010	0.075	0.174	1.239
1.6G0.32C0.36D	0.880	0.948	0.914	0.122	0.037	0.893	−0.157	0.273	0.003	0.040	0.237	1.172
1.6G0.32C0.36D-S	0.912	0.947	0.930	0.126	0.019	0.895	−0.160	0.277	0.002	0.026	0.248	1.000
1.6G0.32C0.40D	0.936	0.979	0.958	0.128	0.022	0.848	−0.149	0.306	0.005	0.049	0.264	1.113
1.8G0.32C0.32D	0.409	0.448	0.429	0.041	0.046	0.895	−0.095	0.226	0.022	0.091	0.174	1.254
1.8G0.32C0.36D	0.464	0.493	0.479	0.047	0.030	0.902	−0.096	0.197	0.004	0.034	0.170	1.264
1.8G0.32C0.40D	0.517	0.534	0.526	0.052	0.017	0.909	−0.096	0.202	0.018	0.071	0.163	1.274
1.2G0.36C0.32D	3.174	3.316	3.245	0.816	0.022	0.957	−0.351	0.468	0.003	0.076	0.376	0.857
1.2G0.36C0.36D	3.625	3.834	3.730	0.978	0.028	1.031	−0.378	0.426	0.007	0.108	0.289	0.924
1.2G0.36C0.40D	3.346	3.596	3.471	0.855	0.036	0.836	−0.307	0.525	0.002	0.049	0.472	0.749
1.4G0.36C0.32D	2.516	2.559	2.538	0.564	0.009	0.988	−0.340	0.399	0.004	0.072	0.311	1.027
1.4G0.36C0.36D	2.736	2.866	2.801	0.636	0.023	0.993	−0.342	0.397	0.008	0.105	0.273	1.032
1.4G0.36C0.40D	2.911	3.080	2.996	0.685	0.028	0.974	−0.336	0.416	0.006	0.094	0.304	1.012
1.6G0.36C0.32D	1.627	1.773	1.700	0.311	0.043	0.920	−0.277	0.357	0.003	0.055	0.297	1.070
1.6G0.36C0.36D	1.777	1.870	1.824	0.336	0.026	0.884	−0.266	0.384	0.009	0.107	0.278	1.028
1.6G0.36C0.40D	2.039	2.143	2.091	0.400	0.025	0.924	−0.278	0.380	0.009	0.102	0.274	1.075
1.8G0.36C0.32D	1.129	1.234	1.182	0.181	0.045	0.937	−0.228	0.300	0.011	0.103	0.201	1.200
1.8G0.36C0.36D	1.209	1.333	1.271	0.196	0.049	0.921	−0.224	0.334	0.037	0.160	0.218	1.178
1.8G0.36C0.40D	1.379	1.458	1.419	0.224	0.029	0.913	−0.222	0.327	0.012	0.097	0.238	1.168

the two values due to the softening term is expected to decrease if the smoothing length is decreased, and that can be done if the number of the particles is increased, although it is not intuitive to state whether the separation found by the geometrical way would increase or decrease. Only one test was made for the CEE study of the formation of the specific binary; a simulation with 200k particles resulted in a 7 per cent smaller final orbital separation than the same case modelled with 100k particles (Nandez et al. 2015). To clarify, the smoothing length was smaller in the case of 200k by 20 per cent compared to the case of 100k, but the relative difference between the final separations derived in the two ways was smaller. The models presented in this study might be affected similarly, but it is likely that the relative change in the final results will be small even if the resolution will be doubled.

Even though the smoothing lengths of the point masses are partially responsible for the discrepancy between the orbital separations found by the two methods, the smoothing length values cannot explain the unbinding of the puffed-up envelope. For instance, let us consider the model mentioned above with the maximum discrepancy of 18 per cent, 1.8G0.32C0.32W. The smoothing lengths for the RG core and WD are $h_{core} = 0.35\,R_\odot$ and $h_{WD} = 0.73\,R_\odot$. The softening in this case starts to work when the distance between the RG core and the WD is $2.16\,R_\odot$. At that moment, most of the mass is located at an average distance of 14 $R_\odot$, except for a few strongly bound particles which remain bound within about 3 $R_\odot$ from the centre of mass. The final separation therefore can be dependent on the mass resolution of the particles that were initially strongly bound and were in the close neighbourhood of the RG core (where the smoothing length becomes important). However, as was discussed previously in Section 4.2, the binary is decoupled with the puffed-up outer envelope, which is too far from the binary to be able to effectively transfer away its orbital energy, and the envelope ejection only depends on the stored kinetic and recombination energy, and does not affect the final parameters of the binary.

Table 3 shows that the bigger the initial mass of the RG, the tighter is the final orbit, for each fixed companion mass. For each initial RG mass and different companion mass, usually, the smaller the mass of the companion, the tighter the final orbital separation. However, there are two exceptions.

(i) In the case of the 1.2 $M_\odot$ RG with a $0.32\,M_\odot$ core, the largest final orbital period is for the $0.36\,M_\odot$ WD companion, instead of the $0.40\,M_\odot$ WD. This could be because the 1.2G0.32C0.36D case deposited the *least* of the kinetic energy in the ejecta, as compared to the other two cases during the spiral-in phase (see Table 2).

(ii) In the case of the 1.4 $M_\odot$ RG with a $0.32\,M_\odot$ core, the tighter final orbit is for the $0.36\,M_\odot$ WD companion instead of the $0.32\,M_\odot$ WD. This could be because the 1.4G0.32C0.36D case deposited more kinetic energy in the ejecta than the other two cases. The final binary in this case also has less remaining bound mass than in the other two cases (see Table 2).

We could not identify any other initial condition that could discriminate why the final orbital separation in the two discussed cases did not follow the trend. During a spiral-in, we find that in those two cases the velocity at which the companion plunges into the envelope was higher than in other cases, which is consistent with the ejecta taking away more angular momentum. However, what causes this deviation in the ejecta's angular momentum is not fully clear.

Fig. 4 shows the final orbital periods for all the simulations, as a function of the initial RG mass. It can be seen that qualitatively there are two populations, mainly defined by the mass of the RG core, and with a smaller dependence on the mass of the companion.

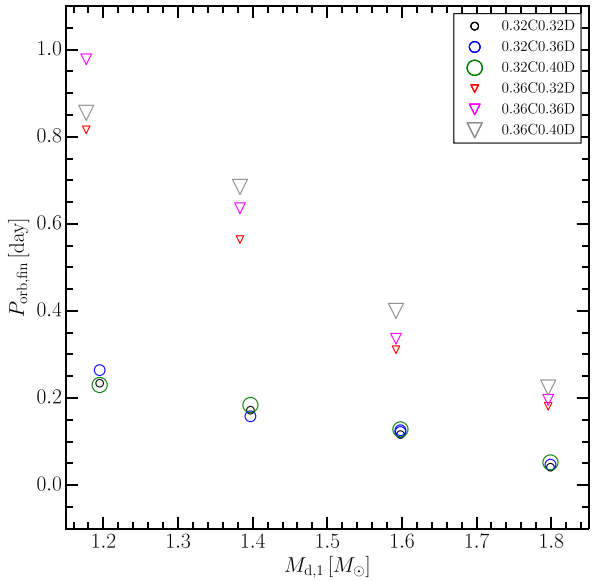

Figure 4. The final orbital periods, plotted against the initial RG mass. The open circles correspond to simulations with $M_{\rm core,1} = 0.32\,{\rm M}_\odot$, while the open triangles correspond to $M_{\rm core,1} = 0.36\,{\rm M}_\odot$. The small, medium, and big symbols are for companions with 0.32, 0.36, and 0.40 $\rm M_\odot$, respectively.

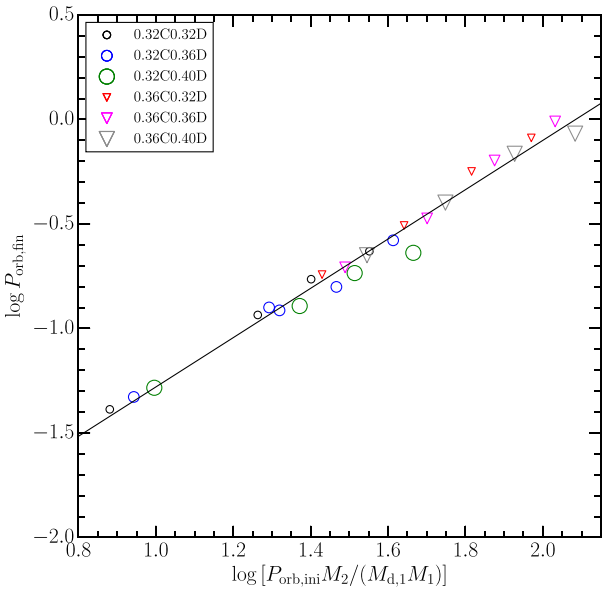

Figure 5. Final orbital periods. This plot contains all non-synchronized simulations. The open circles correspond to simulations with $M_1 \approx 0.32\,{\rm M}_\odot$, while the open triangles correspond to $M_1 \approx 0.36\,{\rm M}_\odot$. The small, medium, and big symbols are for companions with 0.32, 0.36, and 0.40 $\rm M_\odot$, respectively. The black solid line corresponds to the best fit for all the simulations (see equation 14). The orbital periods are in days and the masses are in $\rm M_\odot$.

In each of these two populations, the final orbital period appears to depend almost linearly on the initial RG mass.

Fig. 5 shows the final orbital periods as a function of the initial orbital period, the initial RG mass, the mass of the RG core, and the mass of the companion. This appeared to produce the relationship that can be expressed as follows:

$$P_{\rm orb,fin} = 10^{-2.46\pm0.05}\left(P_{\rm orb,ini}\times\frac{M_2}{M_{\rm d,1}M_1}\right)^{1.18\pm0.04}. \quad (14)$$

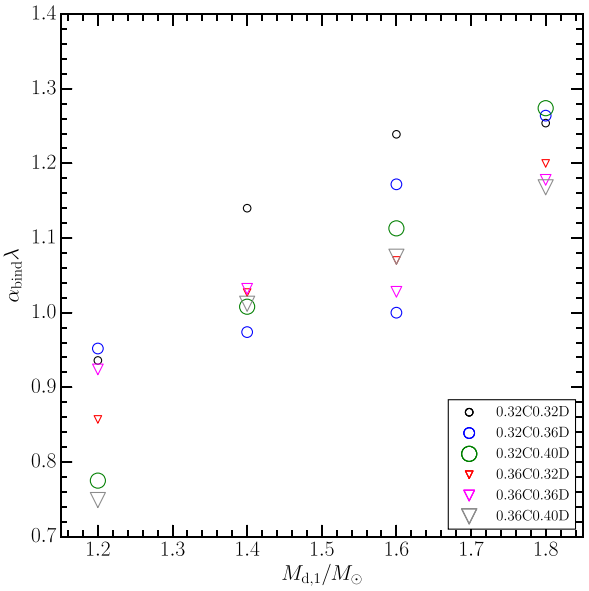

Figure 6. Values for $\alpha_{\rm bind}\lambda$ with respect to the initial RG mass. The open circles correspond to simulations with $M_{\rm c,1} = 0.32\,{\rm M}_\odot$, while the open triangles correspond to $M_{\rm c,1} = 0.36\,{\rm M}_\odot$. The small, medium, and big symbols are for companions with 0.32, 0.36, and 0.40 $\rm M_\odot$, respectively.

Here $\pm$ indicates the standard error for each coefficient. The units for the quantities are $\rm M_\odot$ for all the masses, and days for periods.

4.4 $\alpha_{\rm bind}\lambda$ formalism

In population synthesis models, a crucial parameter is $\alpha_{\rm bind}\lambda$, which can be found from the results of our simulations as follows (see also equation 7):

$$\alpha_{\rm bind}\lambda = -\frac{GM_{\rm d,1}(M_{\rm d,1}-M_{\rm c,1})}{R_{\rm rlof}\Delta E_{\rm orb}}.$$

Note that this quantity does not imply a separate consideration of the recombination energy as it is simply a fit to the standard energy formalism. Fig. 6 shows the behaviour of $\alpha_{\rm bind}\lambda$ in our models. Our best fit for $\alpha_{\rm bind}\lambda$ with the assumed multilinear regression model is

$$\alpha_{\rm bind}\lambda = 0.92 + 0.55\frac{M_{\rm d,1}}{\rm M_\odot} - 0.79\frac{M_2}{\rm M_\odot} - 1.19\frac{M_{\rm c,1}}{\rm M_\odot}. \quad (15)$$

This equation accurately represents all our models, and the maximum deviation between this equation and any data point of 0.13 (1.2G0.32C0.4D), and a minimum deviation of 0.002 (1.8G0.36C0.40D).

4.5 Energy carried away by the ejecta

The total energy carried by the ejecta is not negligible, and is comparable, within an order of magnitude, to the initial binding energy of the RG star. Fig. 7 shows the ratio of the energy taken away by the unbound material to the released orbital energy, $\alpha^\infty_{\rm unb}$. It can be seen that $\alpha^\infty_{\rm unb}$ decreases with the mass of the RG. A multilinear regression that uses all the points from the simulations (assuming that all the variables presented have linear trends with respect to each other) gives the following dependence:

$$\alpha^\infty_{\rm unb} = -\frac{E^\infty_{\rm tot,unb}}{\Delta E_{\rm orb}} = -0.16 - 0.30\frac{M_{\rm d,1}}{\rm M_\odot} + 0.49\frac{M_2}{\rm M_\odot} + 2.27\frac{M_{\rm c,1}}{\rm M_\odot}. \quad (16)$$

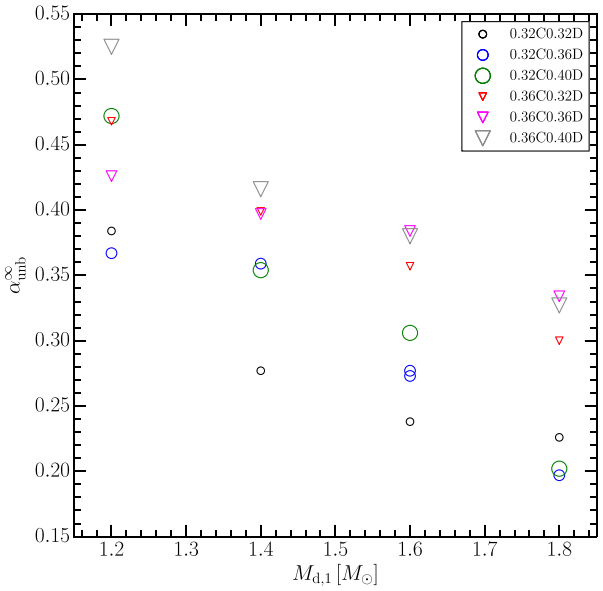

Figure 7. Values for $\alpha^{\infty}_{\rm unb}$ with respect to the initial RG mass. The open circles correspond to simulations with $M_{\rm core,1} = 0.32\,{\rm M}_\odot$, while the open triangles correspond to $M_{\rm core,1} = 0.36\,{\rm M}_\odot$. The small, medium, and big symbols are for companions with 0.32, 0.36, and 0.40 $\rm M_\odot$, respectively.

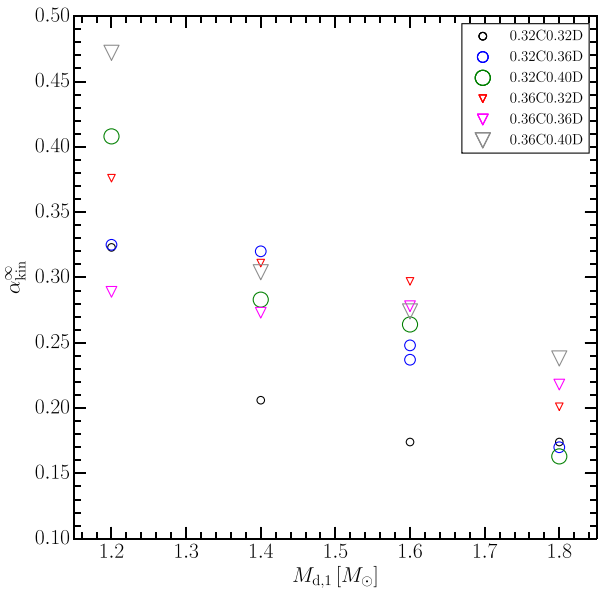

Figure 8. Values for $\alpha^{\infty}_{\rm kin}$ with respect to the initial RG mass. The open circles correspond to simulations with $M_{\rm c,1} = 0.32\,{\rm M}_\odot$, while the open triangles correspond to $M_{\rm c,1} = 0.36\,{\rm M}_\odot$. The small, medium, and big symbols are for companions with 0.32, 0.36, and 0.40 $\rm M_\odot$, respectively.

We note that this equation fits all our models. The maximum deviation between this equation and any point is found to be 0.07 (1.2G0.32C0.40D), and the minimum is 0.005 (1.4G0.36C0.32D).

Table 3 shows $\alpha^{\infty}_{\rm kin}$, which is defined as the ratio of the kinetic energy taken away by the ejecta to the released orbital energy. Fig. 8 shows a monotonic decrease of $\alpha^{\infty}_{\rm kin}$ with the initial mass of the RG, very similarly to $\alpha^{\infty}_{\rm unb}$. The multilinear fitting equation takes the

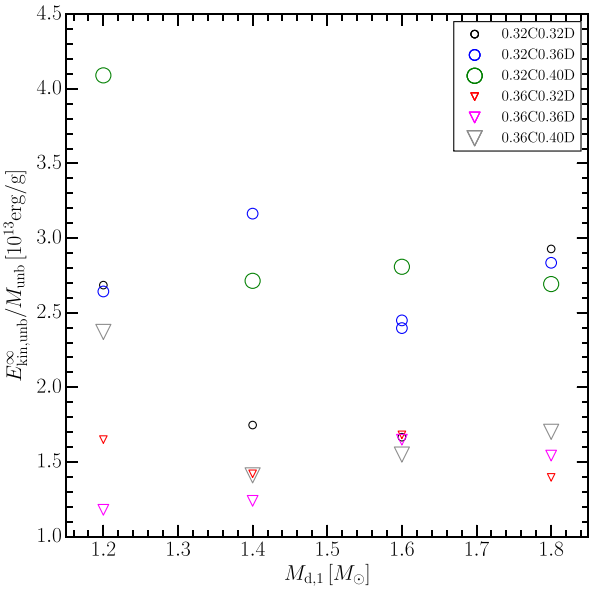

Figure 9. Values for $E^{\infty}_{\rm kin,unb}/M_{\rm unb}$ with respect to the initial RG mass. The open circles correspond to simulations with $M_{\rm c,1} = 0.32\,{\rm M}_\odot$, while the open triangles correspond to $M_{\rm c,1} = 0.36\,{\rm M}_\odot$. The small, medium, and big symbols are for companions with 0.32, 0.36, and 0.40 $\rm M_\odot$, respectively.

following form:

$$\alpha^{\infty}_{\rm kin} = -\frac{E^{\infty}_{\rm kin,unb}}{\Delta E_{\rm orb}} = 0.20 - 0.26\frac{M_{\rm d,1}}{\rm M_\odot} + 0.44\frac{M_2}{\rm M_\odot} + 0.92\frac{M_{\rm c,1}}{\rm M_\odot}, \quad (17)$$

where this equation fits all the points presented in Table 3. The maximum deviation between this equation and any listed value in Table 3 is 0.07 (1.4G0.32C0.32D), while the minimum deviation is 0.0002 (1.2G0.32C0.32D).

The potential energy of the ejecta, compared to the initial potential energy, is not really significant, as in all cases $\alpha_{\rm pot} \lesssim 0.04$. The thermal energy the ejecta still has at infinity, as compared to the initial thermal energy plus the recombination energy, is several times larger, albeit also limited to $\alpha_{\rm th} \lesssim 0.16$. The thermal energy of the ejecta is comparable to the kinetic energy of the ejecta; therefore, the internal energy still plays a role in supporting the ongoing expansion of the material even after all the material is unbound.

Fig. 9 shows how the specific kinetic energy of the ejecta changes with the initial mass of the RG. We can see that overall this energy decreases as the RG mass increases, but no clear trend is observed.

Fig. 10 shows how the sum of the potential and thermal specific energies of the ejecta changes with the mass of the RG. We cannot really see a trend, except that for RGs with the initial mass of 1.8 $\rm M_\odot$, this quantity is higher than for the rest. Note that this quantity is always smaller than the specific kinetic energy of the ejecta.

5 DISCUSSION

To study the formation of a DWD binary via a CEE, we have simulated 25 three-dimensional hydrodynamical interactions between a low-mass RG and a WD companion. We considered for the initial masses of the low-mass RG star 1.2, 1.4, 1.6, or 1.8 $\rm M_\odot$, with a He core of 0.32 or 0.36 $\rm M_\odot$, and WD companions with masses 0.32, 0.36, or 0.40 $\rm M_\odot$. We find that in all the cases, a DWD binary is

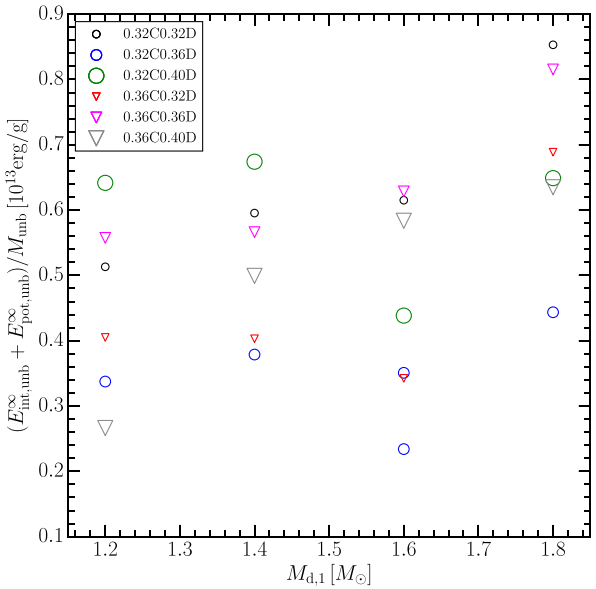

Figure 10. Values for $(E^{\infty}_{\rm int,unb} + E^{\infty}_{\rm pot,unb})/M_{\rm unb}$ with respect to the initial RG mass. The open circles correspond to simulations with $M_{\rm c,1} = 0.32\,{\rm M}_\odot$, while the open triangles correspond to $M_{\rm c,1} = 0.36\,{\rm M}_\odot$. The small, medium, and big symbols are for companions with 0.32, 0.36, and 0.40 $\rm M_\odot$, respectively.

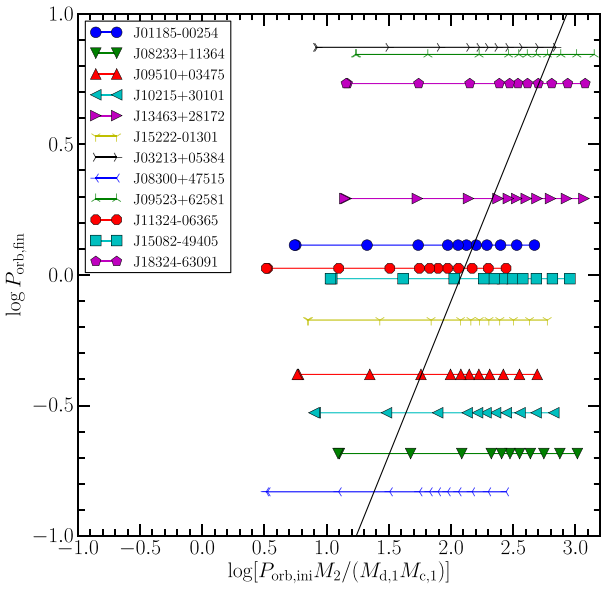

Figure 11. Final orbital periods of sdB stars (from Kupfer et al. 2015) and their pre-CE conditions, as inferred from equation (14). The solid black line is the relation provided by equation (14). The crossing horizontal lines show the positions for different initial donor masses, using observed older WD masses. Solid symbols are for RG donors [zero-age main sequence (ZAMS) masses from 1.0 to 1.8 $\rm M_\odot$ with an increment of 0.1 $\rm M_\odot$, with the lowest mass on the right]. The RG donors are selected when their cores are 0.47 $\rm M_\odot$. Open symbols are for AGB donors (ZAMS masses 1.8, 1.9, and 2.0 $\rm M_\odot$, the smallest on the right). The AGB donors are selected when their cores are 0.53 $\rm M_\odot$.

formed, most of the envelope is ejected, and only a few SPH particles remain bound to the binary in some cases (the bound mass is less than 0.06 per cent of the initial envelope mass). The envelope is ejected on the dynamical time-scale of the expanded envelope.

Our results show that the standard energy formalism should be modified to take into account (i) the energy that is taken away by the ejecta, as it is a substantial fraction of the released orbital energy, and (ii) the recombination energy, which plays a crucial role in ejection of the formed circumbinary envelope. The role of the recombination energy for the CEE with a low-mass RG donor is not that it is necessary for the overall energy budget, as none of the considered systems were expected to merge by the standard energy formalism, but because the recombination occurs exactly at the time when the shrunk binary is no longer capable of transferring its orbital energy to the expanded envelope.

For future population synthesis studies, we provide three ways in which our results can be used.

First of all, we provide a fitting formula (equation 14) that relates the final orbital period, the initial orbital period, the companion mass, the initial RG mass, and the RG core. The RG radius and its core mass are coupled for each donor mass (these can be found using single stellar evolution tracks). The initial RG mass, its radius, and the initial orbital period are also related (e.g. by using the RL radius approximation from Eggleton 1983). Therefore, our fitting formula provides the relation between the observed parameters – the post-CE orbital period and the observed masses of both WDs – and the RG mass and radius before the CE. And vice versa, a population study could use this fitting formula to obtain the post-CE orbital period from known binary parameters at the start of a CE.

Let us consider how this fitting formula can be used to interpret observed post-CE binaries. For example, take the WD 1101+364, which has observed parameters best matching the set of models we have calculated: $P_{\rm orb,fin} = 0.145$ d, $M_1 = 0.31$ $\rm M_\odot$, and $M_2 = 0.36$ $\rm M_\odot$ (Marsh 1995). To find the radius of the donor at the time when it had a core of the same mass as a younger WD in the observed sample, we used parametrized evolutionary tracks from Hurley, Pols & Tout (2000). For WD 1101+364, the fitting formula predicts a pre-CE donor mass of 1.5 $\rm M_\odot$ and a pre-CE orbital period of 33 d. We note that more detailed studies devoted to the simulations specifically of WD 1101+364 gave a similar pre-CE donor mass, 1.5 $\rm M_\odot$ (Nandez et al. 2015). We note that since the pre-CE radius is a strong function of the core mass, uncertainty in the mass of a younger WD leads to a large uncertainty on the pre-CE donor. For example, if the mass is only a bit smaller, $M_1 = 0.29$ $\rm M_\odot$, and the companion's mass is $M_2 = 0.33$ $\rm M_\odot$ (defined by the observed mass ratio of 0.87), then the donor would rather have an initial mass of 1.3$\rm M_\odot$ and a pre-CE orbital period of 26 d.

The second observable type of post-CE binaries for which we can test the fitting equation are hot subdwarf B stars (sdBs). These stars are hot core helium-burning stars with masses around 0.5 $\rm M_\odot$. We note that the post-CE remnants of this mass are beyond the set of our current simulations (modelling a CEE with a more evolved donor requires substantially more GPU time than is available at existing Compute/Calcul Canada facilities, and therefore is not feasible yet), but we will try to look at the post-CE binaries to see if we can place any constraint on their past. We use 12 sdB binaries for which Kupfer et al. (2015) have found orbital periods, and inferred the minimum companion masses in these systems from the assumption of a canonical mass of 0.47 $\rm M_\odot$ for the sdB stars. In Fig. 11, we show the predictions of our fitting formula. In addition to checking RG donors, we also took into account asymptotic giant branch (AGB) donors. A prediction for a post-CE outcome for an AGB donor cannot be fully trusted, as the fitting formula may not work well for them; both λ in the donor's envelope and the fraction of the recombination energy in the total binding energy of the initial

Table 4. sdB binary predictions. $M_{\rm ZAMS}$, $M_{\rm d,1}$, $M_{\rm c,1}$, and M_2 are the ZAMS mass of the donor from our parameter space, inferred initial donor mass right before the CEE, mass of the donor's core (which is assumed to become an sdB star after the CEE), and the companion mass (assumed to be the minimum companion mass from Kupfer et al. 2015), respectively. All the masses are in $M_\odot$. $R_{\rm d,1}$ is the inferred radius of the donor star right before the CEE in $R_\odot$. $P_{\rm orb,ini}$ and $P_{\rm orb,ini}$ are the inferred initial orbital period and the observed orbital period, respectively, in days. Stage is the evolutionary stage of the donor right before the CEE, AGB star, or RG star.

Object	$M_{\rm ZAMS}$	$M_{\rm d,1}$	$M_{\rm c,1}$	$R_{\rm d,1}$	M_2	$P_{\rm orb,ini}$	$P_{\rm orb,fin}$	Stage
J08300+47515	1.80	1.75	0.53	110	0.14	212.03	0.15	AGB
J08233+11364	1.90	1.87	0.53	64	0.44	106.94	0.21	AGB
J10215+30101	1.90	1.87	0.53	64	0.30	100.42	0.30	AGB
J09510+03475	1.80	1.75	0.53	110	0.23	229.56	0.43	AGB
J15222−01301	1.80	1.75	0.53	110	0.27	235.69	0.67	AGB
J15082−49405	1.80	1.75	0.53	110	0.39	250.38	0.97	AGB
J11324−06365	1.30	1.20	0.47	157	0.14	461.31	1.06	RG
J01185−00254	1.40	1.32	0.47	153	0.22	449.81	1.30	RG
J13463+28172	1.70	1.67	0.47	139	0.49	378.87	1.96	RG
J18324−63091	1.30	1.20	0.47	157	0.50	565.64	5.40	RG
J09523+62581	1.30	1.20	0.47	157	0.58	577.70	6.98	RG
J03213+05384	1.00	0.78	0.47	176	0.31	824.86	7.43	RG

envelope are not the same as in the case of a low-mass RG. However, it is important that at least half of the considered sdB binary systems can be better explained by an RG donor.

Table 4 summarizes the possible progenitors for each sdB binary. We note that we list the values for the closest point in Fig. 11, not the exact intersection between the model and the line with constant final orbital period; the donor mass for each case will not change much from the listed value in the table, only the radius of the donor and its initial orbital period will change. We can see from Table 4 or Fig. 11 that the evolutionary stage of the donor star can be associated with the final orbital period. For $P_{\rm orb,fin} \lesssim 1$ d, the donor star is likely a (relatively more massive) AGB star, while for $P_{\rm orb,fin} \gtrsim 1$ d, the donor star is more likely to be a (relatively less massive) RG.

For a second way to use our results – as in the population synthesis studies that use $\alpha_{\rm bind}\lambda$ formalism to find the outcome of a CEE – we supply the parametrization that directly provides the $\alpha_{\rm bind}\lambda$ value, as a function of the initial donor mass, its core mass, and the companion mass. We note that in no case $\alpha_{\rm bind}\lambda > 1.3$, and our maximum $\alpha_{\rm bind} < 1.03$ (we recall that $\alpha_{\rm bind}$ more than 1 implies that an energy additional to the orbital energy was used, in our case it is the recombination energy). Some past population synthesis studies have considered $\alpha_{\rm bind}\lambda = 2$ (see e.g. Toonen, Nelemans & Portegies Zwart 2012) for all CEEs leading to DWD binary formation, but the results of our simulations do not confirm that such a very high value is plausible, at least in the case of CEEs with low-mass RG donors.

And, finally, we give the preferred way to use our results, which is the most trusted method when one wants to extrapolate our result outside of the parameter space we considered. We advise population synthesis studies to use the energy conservation equation that accounts for all energy sinks and sources. In the energy conservation equation, all initially available recombination energy can be used as an energy source. (Note that this statement is not yet fully justified to extend our results for low-mass giants to the case of more massive or more evolved donors, and shall require further studies.) The ejected material can take away 20–40 per cent of the released orbital energy, both as thermal energy and as kinetic energy, and this is an energy loss. It is this energy that powers those luminous red novae which are produced by a CEE (Ivanova et al. 2013b). For these energy losses, we provided a fitting formula. Then the CEE outcomes can be found using the revised energy formalism as follows:

$$(E_{\rm orb,ini} - E_{\rm orb,fin})(1 - \alpha^{\infty}_{\rm unb}) + E_{\rm bind} + \eta(M_{\rm d,1} - M_{\rm c,1}) = 0\,. \quad (18)$$

ACKNOWLEDGEMENTS

JLAN acknowledges CONACyT for its support. NI thanks NSERC Discovery and Canada Research Chairs Program. The authors thank Craig Heinke for checking English in the manuscript. This research has been enabled by the use of computing resources provided by WestGrid and Compute/Calcul Canada.

REFERENCES

de Kool M., 1990, ApJ, 358, 189
Eggleton P. P., 1971, MNRAS, 151, 351
Eggleton P. P., 1972, MNRAS, 156, 361
Eggleton P. P., 1983, ApJ, 268, 368
Gaburov E., Lombardi J. C., Jr, Portegies Zwart S., 2010, MNRAS, 402, 105
Glebbeek E., Pols O. R., Hurley J. R., 2008, A&A, 488, 1007
Han Z., Podsiadlowski P., Maxted P. F. L., Marsh T. R., Ivanova N., 2002, MNRAS, 336, 449
Hernquist L., Katz N., 1989, ApJS, 70, 419
Hurley J. R., Pols O. R., Tout C. A., 2000, MNRAS, 315, 543
Iben I., Jr, Tutukov A. V., 1984, ApJS, 54, 335
Ivanova N., Nandez J. L., 2016, MNRAS, submitted
Ivanova N. et al., 2013a, A&AR, 21, 59
Ivanova N., Justham S., Avendano Nandez J. L., Lombardi J. C., 2013b, Science, 339, 433
Ivanova N., Justham S., Podsiadlowski P., 2015, MNRAS, 447, 2181
Kupfer T. et al., 2015, A&A, 576, A44
Livio M., Soker N., 1988, ApJ, 329, 764
Lombardi J. C., Jr, Holtzman W., Dooley K. L., Gearity K., Kalogera V., Rasio F. A., 2011, ApJ, 737, 49
Marsh T. R., 1995, MNRAS, 275, L1
Nandez J. L. A., Ivanova N., Lombardi J. C., 2014, ApJ, 786, 39
Nandez J. L. A., Ivanova N., Lombardi J. C., 2015, MNRAS, 450, L39
Paxton B., Bildsten L., Dotter A., Herwig F., Lesaffre P., Timmes F., 2011, ApJS, 192, 3
Portegies Zwart S. F., Meinen A. T., 1993, A&A, 280, 174
Toonen S., Nelemans G., Portegies Zwart S., 2012, A&A, 546, A70
Tutukov A. V., Yungelson L. R., 1981, Nauch. Inform., 49, 3
Tutukov A. V., Yungelson L. R., 1988, Sov. Astron. Lett., 14, 265
van den Heuvel E. P. J., 1976, in Eggleton P., Mitton S., Whelan J., eds, Proc. IAU Symp. 73, Structure and Evolution of Close Binary Systems. Reidel, Dordrecht, p. 35
Webbink R. F., 1984, ApJ, 277, 355

This paper has been typeset from a TEX/LATEX file prepared by the author.